# **Iranian Journal of Medical Physics**

ijmp.mums.ac.ir



# Comparing the Influence of Different-Order HIFU Harmonic Superposition on Focal Temperature of Biological Tissue

Hu Dong 1\*, Gang Liu<sup>2</sup>, Xilong Qu<sup>1</sup>

- 1. School of Information Science and Engineering, Changsha Normal University, Changsha 410100, China.
- 2. School of Information Science and Engineering, Xinyu University, Xinyu, 338004, China.

#### ARTICLE INFO ABSTRACT Introduction: While high-intensity focused ultrasound (HIFU) is widely used for non-invasive tumor Article type: Original Paper ablation, current models fail to account for the cumulative energy contributions of nonlinear harmonics (up to the 256th order), significantly limiting treatment precision. This study quantifies the role of harmonic Article history: superposition (1st+2nd+...+256th order) in regulating HIFU-induced focal temperature and establishes an Received: Jun 21, 2025 optimized harmonic combination to enhance clinical parameter design. Accepted: Nov 10, 2025 Material and Methods: A coupled acousto-thermal model, validated against MRI thermometry, was developed by solving the Westervelt equation and Pennes bioheat equation to simulate nonlinear acoustic Keywords: propagation and transient temperature fields in ex vivo porcine muscle under HIFU irradiation. High-Intensity Focused Results: The 1st+2nd+...+128th harmonic superposition model achieved <2.2% error in focal temperature Ultrasound prediction across all tested power levels (80-200 W), with errors of 1.6% at 80 W (48.18 °C simulated vs. 47.96 °C measured), 1.1% at 140 W (66.0 °C vs. 65.31 °C), 1.8% at 160 W (77.78 °C vs. 76.38 °C), and 2.2% at 200 W (82.25 °C vs. 84.11 °C). Mid-order harmonics (2nd–64th) contributed 75–80% of energy Harmonic Temperature Thermal Therapy deposition, while high-order harmonics (>128th, e.g., 256th at 276.48 MHz) exhibited severe attenuation Nonlinear (135× higher than the fundamental wave). The linear propagation model (fundamental frequency only) underestimated temperatures by 4.8-23.9%, highlighting the necessity of nonlinear harmonic inclusion. Conclusion: This work establishes a harmonically optimized framework for HIFU treatment planning, addressing a critical gap in nonlinear acoustic modeling and enabling safer, precision thermal therapy.

► Please cite this article as:

Dong Hu, Liu G, Qu X. Comparing the Influence of Different-Order HIFU Harmonic Superposition on Focal Temperature of Biological Tissue. Iran J Med Phys 2025; 22: 276-286. 10.22038/ijmp.2025.86253.2514.

# Introduction

As a non-invasive treatment method, highintensity focused ultrasound (HIFU) technology has been widely used in fields such as tumor ablation and tissue hyperthermia [1-3]. Previous studies have extensively investigated on the changes in focal temperature during HIFU irradiation. Guntur et al. used numerical simulations to study the effect of temperature-dependent thermal parameters on the temperature increase of liver tissue exposed to HIFU. The The study compared the traditional method (using constant thermal parameters) with different thermal parameters measured different temperatures (e.g., thermal conductivity and specific heat capacity varying with tissue temperature) [4]. The results suggest that temperature-dependent thermal parameters should be considered for accurate temperature prediction during HIFU treatment planning [4]. Wang et al. simulated the nonlinear acoustic field and thermal pattern of phased array HIFU using an angular spectrum method with a second-order operator splitting scheme. The study compared the results with the Khokhlov-Zabolotskaya-Kuznetsov (KZK) equation

experimental data, showing better agreement [5].Tan et al. used numerical simulation to study the effects of dynamic tissue properties on temperature and thermal damage during HIFU thermal therapy. The results showed that dynamic properties have a significant impact on temperature distribution [6]. Wang et al explored the use of frequency chirping to enhance the thermal field and cavitation at the focal point during HIFU ablation. The study used numerical simulation and experimental methods to compare the effects of constant frequency excitation and frequency chirping on temperature rise. The results showed that frequency chirping can significantly enhance temperature rise [7]. Zou et al. used numerical simulation to study the effect of dynamic tissue properties on temperature rise during HIFU scanning treatment. The study compared the temperature distribution under static and dynamic characteristics, the indicating that dvnamic characteristics significantly affect the heating effect [8]. Here, "dynamic tissue properties" specifically denotes temperature-dependent variations in acoustic (e.g., attenuation coefficient, sound velocity) and thermal

<sup>\*</sup>Corresponding Author: Tel: + 86-0731-84036108; Email: weijundong203@outlook.com



parameters (e.g., conductivity, heat capacity), which evolve during HIFU heating due to physicochemical tissue changes [4, 6, 8, 11]. In contrast, this study employs static parameters to isolate harmonic superposition effects. Takagi et al. developed a method for visualizing HIFU-induced temperature rise using a double-layer tissue-mimicking phantom. The method uses microencapsulated thermochromic liquid crystals (MTLCs) with different temperature sensitivities to achieve a wider range of temperature measurements during HIFU exposure [9]. Li et al. explored how thermal relaxation impacts temperature increases in ex vivo tissues during HIFU. They measured the thermal relaxation times of porcine muscle and fat and assessed the Pennes equation, TWMBT, and DPL models. Findings revealed that the DPL model with measured thermal relaxation times offers more precise temperature predictions during HIFU [10]. Dong et al. simulated the effects of temperature-dependent acoustic and thermal parameters on focal temperature and thermal damage in HIFU-irradiated porcine liver tissue. The study compared the results using constant and dynamic acoustic and thermal parameters and showed that dynamic parameters significantly affected focal temperature [11]. Luan et al. proposed a real-time reconstruction method of HIFU focal temperature field based on deep learning. The method uses a multimodal teacher-student model (MMTS) to aggregate data from different modalities and transfer knowledge from the teacher model to the student model, and the result show that the method can accurately reconstruct the temperature field with a maximum temperature error of less than 2.5°C [12].

However, the above studies have not paid enough attention to the contribution of nonlinear harmonics to the formation of focal temperature. During HIFU irradiation, nonlinear effects will occur when sound waves propagate in biological tissues, leading to the generation of high-order harmonics [13]. These harmonics not only change the energy distribution of the sound field, but may also have a significant impact on the temperature field in the focal area. Studies have shown that nonlinear components such as second harmonics and third harmonics can enhance the energy deposition of the sound field in the focal area, thereby affecting the temperature distribution [14]. Varray et al. found that the energy contribution of the second harmonic in the focal area can reach more than 20% of the fundamental wave, significantly increasing the local temperature [15]. In addition, the generation of high-order harmonics is closely related to tissue characteristics, and differences in nonlinear parameters of different tissues may lead to significant changes in harmonic energy distribution. However, the current research on the specific contribution of different-order harmonics to focal temperature and their superposition effects is still relatively limited, especially the mechanism of action of high-order

harmonics is still unclear. Despite advances in HIFU modeling, no prior work has systematically quantified the cumulative contributions of harmonics beyond the 8th order or identified an optimal cutoff for clinical relevance. This gap critically limits the accuracy of temperature prediction, as high-order harmonics (e.g., >64th) exhibit frequency-dependent attenuation that remains uncharacterized in heterogeneous tissues.

The harmonic superposition effect provides a new idea for accurately predicting the focal temperature distribution during HIFU irradiation. By considering the superposition combination of harmonics of different orders, the energy distribution of the acoustic field and the change of the temperature field can be described more accurately, thereby optimizing the HIFU treatment parameters. However, the main challenges faced by current research include: first, the nonlinear mechanism of harmonic generation is complex and difficult to accurately describe by traditional linear models; second, the interaction of harmonics of different orders and their combined impact on the temperature field have not been systematically studied. Solving these problems will help improve the accuracy and safety of HIFU treatment.

This study aims to explore the effects of differentorder harmonics generated during HIFU irradiation on the focal temperature of biological tissues, focusing on the regulation of the harmonic superposition effect on temperature distribution. The key innovation of this study is the first systematic investigation of the influence of the superposition combination of different-order harmonics on the focal temperature, revealing the potential of harmonic superposition in optimizing HIFU treatment parameters. By combining theoretical modeling with experimental verification, this study provides a harmonically optimized superposition model (1st+2nd+...+128th harmonics) as a key strategy to refine HIFU treatment parameters (e.g., power, exposure duration) in clinical settings. This approach balances prediction accuracy and computational efficiency by excluding high-order harmonics (>128th) with negligible energy deposition due to severe attenuation, thereby improving the precision and safety of thermal therapy.

#### **Materials and Methods**

#### Westervelt equation

This study used the Westervelt equation in nonlinear acoustics to describe the propagation of HIFU in biological tissues. The equation was expressed as [16]:

$$\nabla^2 p - \frac{1}{c^2} \frac{\partial^2 p}{\partial t^2} + \frac{\delta}{c^4} \frac{\partial^3 p}{\partial t^3} + \frac{\beta}{\rho c^4} \frac{\partial^2 p^2}{\partial t^2} = 0$$
 (1)

Where p was the sound pressure, d was the sound velocity of the medium, d was the diffusivity of the



sound wave in the tissue, which quantifies the rate of viscous dissipation of acoustic energy in a medium due

to thermoviscous absorption, and  $\delta=2c^3\alpha/\omega^2$ , where  $\omega$  was the frequency of the sound wave vibration and  $\alpha$  was the sound attenuation coefficient of the medium.  $\beta$  was the nonlinear coefficient,  $\beta=1+B/2A$ , and  $\rho$  were the medium density. For the calculation of harmonic components, the numerical solution of equation 1 could be achieved using the frequency domain finite difference method (FDFD) [17]. Using the Fourier series, the sound pressure p was expanded as [18]:

$$p(z,r,t) = \sum_{n=-\infty}^{+\infty} C_n \exp(jn\tau)$$
 (2)

In equation 2, z denoted the axial distance along the acoustic propagation axis, r represented the radial coordinate perpendicular to the acoustic axis, and t was the time variable. Where  $C_n$  represented the complex amplitude of the n th harmonic component.  $C_n$  was calculated as follows [18]:

$$\frac{dC_n}{dz} = -\frac{in\beta}{2c^3\rho} \sum_{k=-\infty}^{\infty} C_k C_{n-k} + i\frac{c}{4\pi f_0 n} \Delta_{\perp} C_n$$

$$-(\alpha(nf_0) - i\frac{2nf_0}{(\eta - 1)\pi f_*} (\alpha(nf_0) - \alpha(f_0)))C_n$$
(3)

In equation 3,  $f_0$  denoted the fundamental frequency;  $\alpha(nf_0)$  was the sound attenuation coefficient corresponding to n times the fundamental frequency;  $f_*$  was a dimensionless normalized frequency coefficient; and  $\eta$  represented the dimensionless viscosity coefficient of the medium [18]. While equation 2 formally included harmonics of infinite orders ("n"  $\rightarrow \pm \infty$ ), the physically achievable harmonic spectrum in tissue was constrained by two factors: (1) the nonlinear coefficient ( $\beta$ ) of the medium, which governed energy transfer efficiency from the fundamental wave to higher harmonics; and (2) frequency-dependent attenuation (  $\alpha \propto f^2$  ), which exponentially dissipated high-frequency Consequently, harmonics beyond a tissue-specific cutoff order (e.g., >128th in porcine muscle) could not propagate to the focal region due to severe attenuation (e.g., 135× higher for the 256th harmonic vs. fundamental). Thus, although our model computed harmonics up to the 256th order by varying "n", the number of harmonics contributing significantly to focal

heating was intrinsically determined by tissue properties—not arbitrarily selectable.

For benchmarking, a linear propagation model (fundamental frequency only) was implemented, wherein the Westervelt equation (Equation 1) was simplified by omitting nonlinear terms (i.e., setting  $\beta$  = 0). This model assumed purely linear acoustic propagation of the fundamental wave (1.08 MHz) without harmonic generation. The resulting pressure field was used in the Pennes equation (Equation 4) to compute temperature. In contrast, the full nonlinear model (Equation 1–3) incorporates harmonics up to the 256th order.

### Pennes bioheat equation

The temperature distribution in biological tissues was described by the Pennes bioheat equation, which had the form [19,20]:

$$\rho c_t \frac{\partial T_t}{\partial t} = k_t \nabla^2 T_t - w_b c_b (T - T_b) + Q \tag{4}$$

In formula (4), T represented tissue temperature,  $C_t$  and  $k_t$  represented the specific heat capacity and thermal conductivity of biological tissue respectively, and  $W_b$  represented the blood perfusion rate of non-biological tissue. In this study, blood perfusion rate was set to zero as experiments used ex vivo porcine muscle tissue, which lacks active perfusion, so the blood perfusion rate could be ignored in the model and  $W_b = 0$ . This constituted a boundary condition for the ex vivo model, consistent with experimental validation protocols [21].  $C_b$  represented specific heat capacity,  $T_b$  was blood temperature, and Q was ultrasonic power loss. Q could be expressed as [17]:

$$Q = \frac{2\alpha_n}{\omega^2 \rho c} \left\langle \left(\frac{\partial p}{\partial t}\right)^2 \right\rangle \tag{5}$$

In the above formula,  $\alpha_n$  was the attenuation coefficient corresponding to the n th harmonic component, and the symbol  $\langle \ \rangle$  represented the time average value.

#### Quantification of Harmonic Energy Contributions

The percentage energy contribution of each harmonic order n was calculated by decomposing the total absorbed power density Q (Equation 5) into harmonic-specific components. For the n th harmonic, the time-averaged power density  $Q_n$  was given by [22]:



$$Q_{n} = \frac{2\alpha_{n}}{\omega^{2}\rho c} \left\langle \left(\frac{\partial p_{n}}{\partial t}\right)^{2} \right\rangle \tag{6}$$

Where  $P_n$  was the acoustic pressure of the n th harmonic derived from the spectral decomposition in Equation 2. The relative contribution (%) of the n th harmonic to total energy deposition at the focal point was then computed as [15]:

$$Contribut\dot{\boldsymbol{o}}\boldsymbol{n}_{n} = \frac{Q_{n}}{\sum_{k=1}^{N} Q_{k}} \times 100\%$$
(7)

Where N was the maximum harmonic order considered (e.g., N =128 or 256). This formulation accounted for frequency-dependent attenuation ( $\alpha_n \propto f^2$ ) and nonlinear pressure coupling, enabling precise attribution of energy deposition to individual

#### Two-dimensional model of HIFU irradiation

The ultrasonic transducer was a flat, spherically focused circular plane with an outer radius of a = 4cm and a focal length of F = 12cm. The ultrasonic wave propagates in water at a distance of  $z_w = 9$ cm and was irradiated to a porcine muscle tissue with a thickness of  $z_m$  =5cm. It was assumed that the porcine muscle tissue was a uniform medium. Consistent with the ex vivo experimental conditions, blood perfusion effects were omitted ( $^{W_b} = 0$ ). The ultrasonic frequency was  $^f$  =1.08MHz, and the continuous irradiation time of HIFU was 30 seconds. The time step was  $\Delta t = 0.1 \mu s$ , and the grid resolution was  $\Delta x = 0.5$ mm. The coordinate system was centered on the focus and is symmetrically distributed along the acoustic axis (Z direction). The irradiation powers (80W, 140W, 160W, and 200W) were selected to cover clinically relevant intensity ranges for HIFU ablation [21]. The coupled Westervelt and Pennes equations were solved numerically using MATLAB R2018b (The MathWorks, Inc., USA). The Westervelt equation (Equation 1) was discretized in the frequency domain via the finite difference method (FDFD) [17]. Harmonic amplitudes  $C_n$  (for n=1 to

256) were computed sequentially along the axial direction z using Equation 3. The computed acoustic energy deposition Q (Equation 5) served as the heat source in the Pennes bioheat equation (Equation 4), which was solved using an explicit finite difference scheme with a time step of  $\Delta t = 0.1$  µs. Boundary conditions included: (1) Absorbing boundary conditions at radial edges to minimize reflections; (2) Continuity of pressure and particle velocity at the water-tissue interface; (3) Thermal insulation (zero heat flux) at all external boundaries. Initial conditions were set to uniform temperature (20 °C) and zero acoustic pressure throughout the domain. The acoustic and thermal solutions were coupled by updating  $\mathcal Q$  at each time step based on the harmonic amplitudes and then solving the temperature field. During the HIFU irradiation process, the acoustic field and temperature field of biological tissue were coupled and affected by each other. The acoustic-thermal coupling was implemented by sequentially solving the Westervelt equation for harmonic propagation and the Pennes equation for heat

transfer, with Q (Equation 5) coupling the acoustic energy to thermal effects. While this coupling framework followed established principles [8], our implementation in MATLAB uniquely resolved harmonics up to the 256th order and incorporated frequency-dependent attenuation for each harmonic. The two-dimensional model of HIFU irradiated porcine muscle tissue was shown in Figure 1 below:

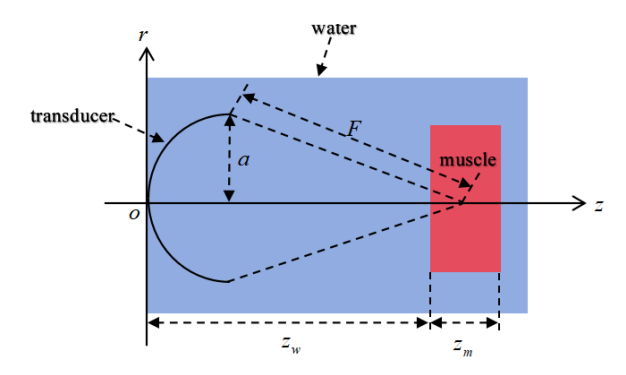


Figure 1. HIFU irradiated porcine muscle model

The acoustic and thermal parameters of water and porcine muscle were shown in Table 1 [21]. All parameters in Table 1 remained constant during simulations, representing baseline values at 20 °C. Although temperature-dependent dynamic properties significantly affect HIFU treatments in vivo [8, 11], this study isolated harmonic superposition effects by fixing parameters. This ensured focal temperature changes were solely attributable to nonlinear acoustic energy cascading.

## MRI Thermometry Validation

To validate the simulated focal temperature, experimental data from Magnetic Resonance Imaging (MRI) thermometry [21] were utilized. The MRI experiments were conducted using a 1.5 T Siemens Symphony scanner with a spoiled gradient echo sequence (TR = 13 ms, TE = 7 ms, flip angle = 30°, slice thickness = 8 mm). Temperature mapping was based on the proton resonance frequency (PRF) shift method, which measures phase differences between preheated and heated states.



Table 1. Acoustic and thermal parameters of the medium

Material	$\rho(kg/m^3)$	c(m/s)	α(Np/m)	B/A	c <sub>t</sub> (J/kg/K)	k <sub>t</sub> (W/m/K)
Water	1000	1520	0.026	5.0	4200	0.60
muscle	1055	1550	4.500	7.0	3200	0.49

The PRF shift method relied on the linear dependence of the proton resonance frequency on temperature (approximately -0.01 ppm/°C for aqueous tissues). Phase differences between baseline (presonication) and heated states were converted to temperature changes using the relation [23]:

$$\Delta T = \frac{\Delta \phi}{\gamma \theta B_0 T E} \tag{8}$$

where  $\Delta\phi$  was the phase shift,  $\gamma$  was the gyromagnetic ratio,  $\theta$  was the PRF coefficient (-0.01 ppm/°C),  $B_0$  was the static magnetic field strength, and TE was the echo time. The temperature uncertainty of this method was  $\pm 1.5$ °C, as reported in [21]. The spatial resolution of MRI was 2 mm per pixel, and temporal resolution was 1.7 s per frame. The HIFU transducer parameters and tissue properties (ex vivo porcine muscle) in [21] were matched with our simulation setup (Table 1), ensuring direct comparability.

#### Data Comparison Protocol

To ensure consistency between simulated and experimental temperatures, the following steps were adopted:

**Data Extraction**: MRI-measured temperature profiles were digitized using calibrated axes, with peak focal temperatures extracted at each power level (80–200 W) [21]. Three independent trials were averaged to minimize experimental variability.

**Spatial Alignment**: Simulated and experimental datasets were spatially aligned to the focal coordinates (axial: z-axis, radial: r-axis), with temperature values normalized to the baseline (20 °C).

**Error Quantification**: Percentage errors between simulated and experimental peak temperatures were calculated as [21]:

$$Error(\%) = \left| \frac{T_{sim} - T_{exp}}{T_{exp}} \right| \times 100$$
(9)

where  $T_{sim}$  and  $T_{exp}$  denoted the simulated and MRI-measured peak temperatures, respectively.

#### Results

The MRI-measured temperature profiles were digitized using calibrated axes and averaged over three repeated trials to minimize experimental variability [21]. The peak focal temperatures at each power level (80–200 W) were extracted with a precision of  $\pm 0.5$ °C, as validated against the original data tables in [21]. By comparing the numerical

simulation results with the MRI measured temperature data [21], which were acquired under identical HIFU parameters (power levels: 80–200 W, exposure time: 30 s) and tissue properties. The focal temperature peaks were extracted following the Data Comparison Protocol described in Section 2.3 (using digitization of MRI profiles, spatial alignment to focus, and voxel-averaging over a volume of  $2 \times 2 \times 8$  mm<sup>3</sup>, consistent with the spatial resolution limitations of the clinical protocol. The effects of different HIFU irradiation powers (80W, 140W, 160W, 200W) and harmonic superposition combinations on the simulated temperature and measured temperature of the porcine muscle tissue focus were systematically analyzed. In Figures 2-5, the time axis (horizontal) denoted seconds elapsed since HIFU initiation. All simulations and experiments span 120 seconds: 0-30 s (active irradiation) and 30-120 s (post-sonication cooling). This captured both energy deposition during sonication and thermal relaxation thereafter, with peak temperatures occurring at t=30 s (end of irradiation) as shown in the transient profiles. The results showed that the superposition effect of nonlinear harmonics significantly regulated the energy deposition and temperature distribution in the focal area, and the effects of different harmonic orders showed a complex pattern. In the following four simulation figures, 1st, 2nd, 3rd, 4th, ..., 256th represented the fundamental wave, second-order harmonic, third-order harmonic, fourth-order harmonic ..., and 256th order harmonic, respectively. At 80W power (Figure 2), the simulated temperature peak of the linear propagation model (fundamental frequency only) was 45.66 °C, which was 2.30 °C different from the MRI measured value (47.96 °C) (error rate 4.8%).

As the harmonic order increased, the temperature showed a non-monotonic trend of first increasing and then decreasing: the peak temperature of the 1st+2nd+...+4th order harmonic combination reached 72.97 °C (error rate 52.1%), indicating potential energy over-focusing, while the temperature of the 1st+2nd+...+128th order combination droped to 48.18 °C, which was only 0.22 °C different from the measured value (error rate 1.6%), and the prediction accuracy was significantly improved. When superimposed on the 256th order harmonic, the temperature further droped to 47.11 °C (error rate 1.8%), but the strong attenuation of high-frequency harmonics (the attenuation coefficient of the 256th order harmonic was 135-fold higher than that of the fundamental wave) may lead to instability of energy deposition. When the power was increased to 140W (Figure 3), the error between the simulated temperature of the fundamental wave (linear propagation) (57.96 °C) and the measured value (65.31 °C) was 11.3%.

The temperature peak of the 1st+2nd+...+4th order harmonic combination abnormally rose to 125.1 °C (error



rate 91.5%), indicating that low-order harmonics may cause local energy over-focusing at high power. The temperature of the 1st+2nd+...+128th order combination

was 66.0 °C, and the error rate was reduced to 1.1%, verifying its reliability.

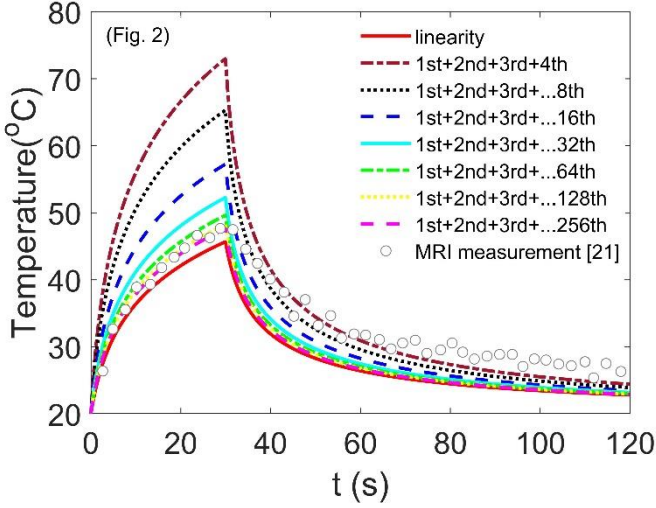


Figure 2. Comparison of simulation and experimental temperature of different order harmonic superposition under 80W HIFU irradiation

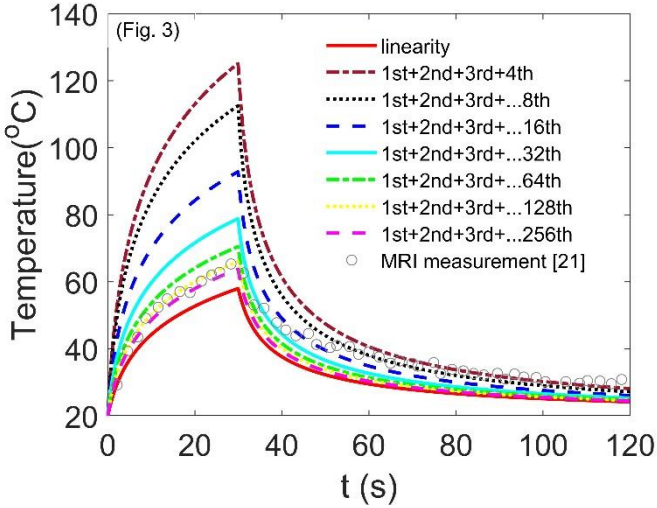


Figure 3. Comparison of simulation and experimental temperature of different order harmonic superposition under 140W HIFU irradiation

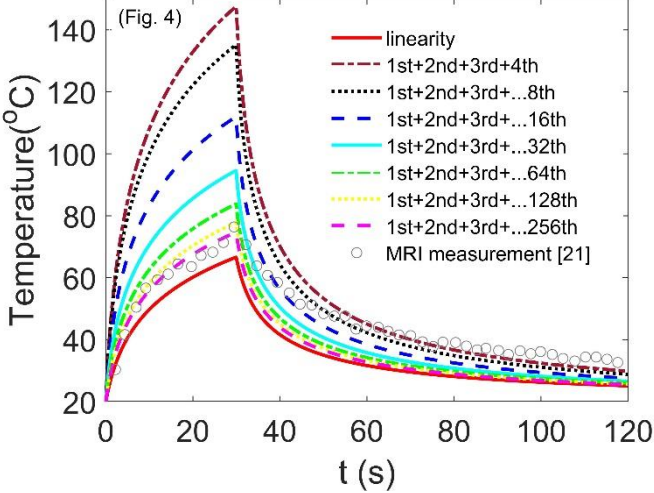


Figure 4. Comparison of simulation and experimental temperature of different order harmonic superposition under 160W HIFU irradiation



When superimposed on the 256th order harmonic, the temperature droped to  $63.72~^{\circ}\text{C}$  (error rate 2.4%), but the attenuation effect of high-order harmonics weakened the energy transfer efficiency. Under high power 160W conditions (Figure 4), the simulated temperature of the fundamental wave (linear propagation) (66.59  $^{\circ}\text{C}$ ) differed by 12.8% from the measured value (76.38  $^{\circ}\text{C}$ ).

The temperature peak of the 1st+2nd+...+4th order combination was as high as 147.5 °C (error rate 93.0%), while the temperature of the 1st+2nd+...+128th order combination was 77.78 °C, and the error rate was reduced to 1.8%, indicating that the low- and medium-order harmonics (2nd~64th order harmonics) contribute about 75% of the energy deposition. This 75-80% represented the proportion of total absorbed acoustic energy attributed to harmonics 2-64 within the 1st-128th harmonic ensemble. Crucially, models truncated at lower orders (e.g., 1st+2nd+...+4th) redistribute this energy unrealistically: while their cumulative absorption may mathematically approach 100% of included harmonics, the exclusion of higher-order components distorts the spatial deposition profile, causing over-concentrated heating at superficial depths (Figure 5). Thus, absolute temperature predictions require balanced inclusion of harmonics 1-128 to accurately resolve the focal energy distribution. When superimposed on the 256th order harmonic, the temperature droped to 74.65 °C (error rate 2.3%), reflecting the limitation of the energy deposition by the cumulative attenuation of high-frequency harmonics (>128th order). At the highest power of 200W (Figure 5), the error rate between the simulated temperature of the fundamental wave (linear propagation) (64.02 °C) and the measured value (84.11 °C) was as high as 23.9%.

The temperature peak of the 1st+2nd+...+4th order combination abnormally rose to 183.9 °C (error rate 118.6%), while the temperature of the 1st+2nd+...+128th order combination was 82.25 °C, with an error rate of 2.2%, highlighting its applicability at high power. When superimposed on the 256th order harmonic, the

temperature droped to 76.13 °C (error rate 9.5%), and the strong attenuation of the high-frequency harmonic (276.48 MHz) caused the energy to be unable to be effectively transferred to the focal area. This reduction occured despite the theoretical generation of high-order harmonics because frequencies >138 MHz (e.g., 256th at 276.48 MHz) exhibit attenuation coefficients exceeding 250,000 Np/m in muscle

tissue (  $\alpha_{muscle} = 4.5 \times (f/1.08)^2$  ), restricting penetration to <0.2 mm. Thus, while nonlinear propagation generated these harmonics, their energy was deposited superficially rather than at the focus, reducing net focal heating.

Comprehensive analysis showed that the 1st+2nd+...+128th harmonic combination exhibited the best prediction accuracy (average error rate of 1.9% across 80-200 W) at different powers. Its advantage came from the comprehensive coverage of the energy contribution (about 80%) of medium and low-order harmonics (2nd~64th order harmonics), while avoiding the excessive attenuation effect of high-order harmonics (>128th order) (for example, the attenuation coefficient of 138MHz harmonics was 135 times that of the fundamental wave). The superposition of low-order harmonics (such as 2nd~4th order harmonics) caused abnormal temperature rise under high pressure, which might have been related to the local energy focusing of low-frequency harmonics, whereas the superposition of high-order harmonics (>256th order) led to a decrease in energy deposition efficiency due to the reduced penetration depth.

The 1st+2nd+...+128th order harmonic superposition model achieved high-precision temperature prediction by balancing energy contribution and attenuation effect, providing a theoretical basis for the optimization of HIFU treatment parameters. Notably, beyond the irradiation endpoint (t > 30 s), all models—including the fundamental wave-only and truncated harmonic combinations — converged during the cooling phase (Figs. 2-5).

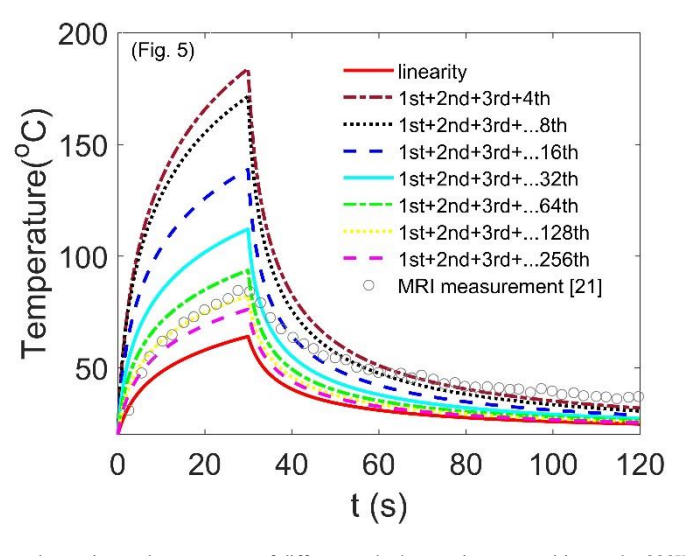


Figure 5. Comparison of simulation and experimental temperature of different order harmonic superposition under 200W HIFU irradiation



This occured because temperature decay was governed exclusively by thermal diffusion (Equation 4), independent of acoustic energy deposition ( $\mathcal{Q}=0$  after sonication). Thus, while higher-order harmonics (e.g., 128th) were critical for accurate peak temperature prediction at t = 30 s, their exclusion did not alter cooling dynamics.

#### Discussion

This study revealed the influence mechanism of different harmonic superposition orders on HIFU focal temperature and its difference with the actual MRI measured value through systematic comparison of numerical simulation and experimental data.

The average error rate between the simulated temperature and the MRI measured value of the 1st+2nd+...+128th order harmonic combination was stable within 2.2% across all tested power levels (80-200 W), with a slight increase to 2.2% at 200 W due to high-frequency attenuation. Its high accuracy came from the precise balance between energy contribution and attenuation boundary. The low- and medium-order harmonics (2nd to 64th order harmonics) contribute about 80% of the total energy deposition, of which the second harmonic accounted for 18% to 22%, and the third to eighth order harmonics contributed a cumulative 15% to 20%. These harmonics had moderate frequencies (2.16 to 8.64MHz) and low attenuation coefficients, which could effectively penetrate into the focal area and achieve efficient energy deposition [24-26]. At the same time, the 128th harmonic frequency (138 MHz) approached the practical penetration limit for therapeutic ultrasound in biological tissues, where

the attenuation coefficient (  $\alpha \approx 4.5 \times (138/1.08)^2$ =73,500 Np/m) reduced energy penetration to <1 mm. Consequently, harmonics beyond this frequency (e.g., 256th at 276.48 MHz,  $\alpha \approx 291,600 \text{ Np/m}$ ) deposit >99.9% of their energy superficially, failing to reach the focal zone. This combination not only covered the main energy contribution harmonics, but also avoided the excessive attenuation of high-order harmonics, thereby optimizing the prediction accuracy. Recent studies (e.g., Mortazavi et al. [27]) have similarly validated HIFU models using pre-existing experimental demonstrating that nonlinear harmonic effects significantly alter focal heating patterns. Our work extended this approach by systematically analyzing harmonics up to the 256th order, whereas prior studies typically truncate at lower orders (e.g., 8th harmonic). The close agreement (<2.2% error) between our 1st-128th harmonic model and MRI data [21] underscored the necessity of including mid-order harmonics (2nd+...+64th) for clinical relevance. The distinct heating effects of low- and high-order harmonics arise from their frequency-dependent energy deposition and attenuation. Low-order harmonics (2nd+...+8th) exhibit moderate frequencies (2.16-8.64 MHz) and attenuation coefficients (e.g., 9.72 Np/m for 2nd harmonic at 2.16 MHz in muscle), enabling deeper penetration and

cumulative energy deposition. For instance, the second harmonic contributes 18–22% of the total absorbed power (Figure 3), enhancing focal heating via nonlinear energy transfer from the fundamental wave. In contrast, high-order harmonics (>64th, e.g., 138 MHz for 128th harmonic) suffer severe attenuation (135× higher than the fundamental wave) due to the frequency-squared

dependence of absorption (  $\alpha \propto f^2$  ), limiting their penetration depth and causing rapid energy dissipation. This attenuation shifted energy deposition toward superficial regions, reducing focal temperature rise. Mid-order harmonics (8th+...+64th) strike a balance, contributing 15-20% cumulative energy without excessive attenuation, thereby dominating the focal heating process. Critically, while our computational framework evaluated harmonics up to the 256th order (by incrementing "n" in Equation 2), the effective harmonic spectrum in tissue is physiologically capped by attenuation and nonlinearity—highlighting that tissue properties, not computational choice, dictated the viable harmonic orders. The apparent paradox—where higher harmonic inclusion reduced focal temperature despite their theoretical energy contribution (10-15%)stemmed from the exponential decay of high-frequency waves in tissue. For instance, the 256th harmonic (276.48 MHz) experienced attenuation 135× higher than the fundamental wave (Figure 5), depositing >99.9% of its energy within 1 mm of the transducer surface. This energy never reached the focus, explaining the temperature decrease. Crucially, MRI thermometry [21] confirmed this attenuation-limited behavior: focal temperatures align only with models that exclude harmonics above 128th (138 MHz),

 $\alpha \approx 4.5 \times (138/1.08)^2$  =73,500 Np/m still permited partial focal penetration. The apparent temperature overestimation by mid-order harmonics (e.g., 2nd-64th) in truncated models arised from unphysical energy localization, not excessive total deposition. When harmonics >64th were excluded, the unresolved nonlinear energy cascade forced excessive power density near the transducer face (Figure 5, 1st+...+4th curve). This violated the diffraction-governed focal geometry, artificially inflating focal temperatures despite similar cumulative absorption percentages. In contrast, the 1st-128th ensemble correctly distributed energy across harmonics, with mid-order components (2nd-64th) depositing 75-80% of the total focal energy - consistent with their moderate attenuation and optimal penetration depth.

In contrast, low-order combinations (such as 1st+2nd+...+4th order) ignored the cumulative contribution of high-order harmonics (about 10%~15%), resulting in a temperature prediction error rate of 52%~119%; while high-order combinations (such as 1st+2nd+...+256th order) had a significant increase in error rate (such as 9.5% at 200W) due to severe energy loss. This comparison highlighted the key role of harmonic order selection in model design. The transient



temperature profile (e.g., peak at 30 s followed by decline) resulted from competing thermal processes: (1) Initial rapid heating due to cumulative energy deposition from low- and mid-order harmonics (2nd+...+64th), which dominate within the first 30 s; (2) Subsequent

cooling driven by thermal diffusion (governed by  $k_{\scriptscriptstyle t}$ 

=0.53 W/m/K) and the absence of blood perfusion ( $^{W_b}$  =0) in the ex vivo model. This simplification aligned with the non-perfused nature of ex vivo tissues. Beyond 30 s, heat dissipation to surrounding tissue outweighed harmonic energy deposition, particularly as high-order harmonics (>128th) attenuate rapidly and fail to sustain focal energy input. Particularly as high-order harmonics (>128th) attenuate rapidly and fail to sustain focal energy input. Crucially, once irradiation ceased (t > 30

s), the ultrasonic power loss term  $\mathcal{Q}$  vanishes (Equation 5), and temperature evolution became purely thermal diffusion-driven. This explained why models with divergent harmonic orders converge during cooling (Figs. 2-5): diffusion depends only on tissue

conductivity ( $^{k_t}$ ), density ( $^{\rho}$ ), and heat capacity ( $^{c_t}$ ), not acoustic energy sources. Consequently, while midorder harmonics (2nd-64th) dictate peak heating, their exclusion does not affect post-sonication cooling accuracy. As shown in Figure 5, this phenomenon was amplified at higher powers (e.g., 200 W), where faster initial heating exacerbates thermal diffusion losses.

propagation model (fundamental The linear frequency only) seriously underestimated temperature at all powers (error rate 4.8%~23.9%). The fundamental reason was that it completely ignored the energy cascade effect of nonlinear harmonics. In the actual HIFU sound field propagation, nonlinear effects lead to the generation of harmonics, which significantly increased the total absorbed power by transferring energy from the fundamental wave to higher-order harmonics [28,29]. For example, the sound pressure amplitude of the second harmonic can reach 10%~15% of the fundamental wave, and its energy density contribution exceeds 20%. The linear model did not take into account the energy of harmonic superposition,

resulting in Q being seriously underestimated. In addition, the nonlinear coefficient of porcine muscle was significantly higher than that of water, which further amplified the impact of nonlinear effects on temperature, and the linear model could not reflect this tissue-specific parameter difference.

Although the 1st+2nd+...+128th order combination showed high prediction accuracy, we still need to pay attention to the following potential sources of error: First, the simulation assumed that porcine muscle tissue was a homogeneous medium, while the acoustic

parameters of actual tissue (such as  $\alpha$ ,  $\beta$ ) might have spatial heterogeneity, which affected the harmonic energy distribution; second, the current model did not consider the nonlinear interaction between harmonics

(such as harmonic-harmonic coupling), which might introduce small errors at high power (such as an error rate of 2.2% at 200 W).

Future research needs to further quantify tissue heterogeneity and high-order harmonic attenuation mechanisms through multi-physics field coupling models (integrated acoustic field, temperature field and tissue damage dynamics) and high-frequency acoustic imaging technology. For example, for the acoustic-thermal coupling effect of harmonics >256, it is necessary to combine experimental measurements of their actual penetration depth and energy deposition efficiency to improve the boundary condition assumptions of the model.

The strong attenuation of high-order harmonics and the nonlinear energy cascade effect were the core mechanisms for temperature distribution regulation. The 1st+2nd+...+128th order combination achieved high-precision temperature prediction by balancing energy contribution and attenuation boundaries. Model optimization needed to focus on tissue-specific parameter quantification and high-order harmonic interaction mechanism analysis to promote the precision of HIFU treatment parameters and the safety of clinical applications.

#### Conclusion

This study systematically reveals, for the first time, the cumulative influence of harmonic superposition (up to the 256th order) on focal temperature in highintensity focused ultrasound (HIFU)-irradiated porcine muscle tissue by establishing a coupled acousto-thermal model integrating the Westervelt equation and the Pennes bioheat equation. Numerical simulations validated against MRI thermometry demonstrate that the proposed model (1st+2nd+...+128th)superposition) achieves exceptional accuracy (average error rate 1.9%, maximum 2.2% at 200 W) in focal temperature prediction across clinically relevant power levels (80-200 W), significantly outperforming linear models (4.8-23.9% error). The model's superiority stems from its balanced inclusion of mid- and low-order harmonics (2nd-64th), which collectively contribute 75-80% of total energy deposition, while excluding higher-order harmonics (>128th) that suffer severe frequency-dependent attenuation. For instance, the 128th harmonic (138 MHz) exhibits an attenuation coefficient 135× higher than the fundamental wave (1.08 MHz), leading to negligible energy transfer to the focal region.

In contrast, truncating harmonics at lower orders (e.g., 4th) caused severe overestimation (91.5% error at 140 W) due to unaccounted energy cascading, whereas excessive inclusion (e.g., 256th) introduced underestimation (9.5% error at 200 W) from high-frequency dissipation—both scenarios posing risks of overtreatment or undertreatment in clinical settings. The linear model's consistent underestimation (4.8–23.9% error) underscores the critical role of nonlinear energy cascading, where harmonic generation transfers energy



from the fundamental wave to higher frequencies, amplifying focal heating beyond linear predictions.

These findings establish a harmonically optimized framework for HIFU treatment planning. Future work should prioritize (1) multi-physics modeling of tissue heterogeneity's impact on harmonic attenuation, (2) experimental characterization of ultra-high-frequency harmonics (>256th) in vivo to validate attenuation physics at extreme frequencies and explore potential applications in superficial micro-therapies, where their confined energy deposition may be advantageous, and (3) integration with real-time thermometry to advance clinical translation.

#### Acknowledgment

This work was supported by the Key Project of Hunan Provincial Department of Education of China under grant No. 21A0618, and the Project of Ministry of Education Humanities and Social Sciences Research Youth Fund No. 22YJCZH025. The authors sincerely thank the anonymous reviewers for their helpful comments and suggestions.

#### References

- Wessapan T, Keangin P, Rattanadecho P, Somsuk N. Comparative analysis of heat transfer dynamics in high-intensity focused ultrasound and microwave ablation for cancer treatment. International Journal of Thermofluids. 2025 Mar 1;26:101090. doi:10.1016/j.ijft.2025.101090.
- Rohfritsch A, Barrere V, Estienne L, Melodelima D. 2D ultrasound thermometry during thermal ablation with high-intensity focused ultrasound. Ultrasonics. 2024 Aug 1;142:107372.
- 3. Cambronero S, Dupré A, Mastier C, Chen Y, Hamelin O, Melodelima D. Intraoperative HIFU ablation of the liver at the hepatocaval confluence as adjunct to surgery: Preliminary animal experiments. Ultrasonics. 2025 Apr 1;148:107556.
- 4. Guntur SR, Choi M. Influence of temperature-dependent thermal parameters on temperature elevation of tissue exposed to high-intensity focused ultrasound: numerical simulation. Ultrasound Med Biol. 2015;41(3):806-13. doi:10.1016/j.ultrasmedbio.2014.10.008.
- Wang M, Zhou Y. Simulation of non-linear acoustic field and thermal pattern of phased-array highintensity focused ultrasound (HIFU). Int J Hyperthermia. 2016;32(5):569-82. doi:10.3109/02656736.2016.1160154.
- Tan Q, Zou X, Ding Y, Zhao X, Qian S. The influence of dynamic tissue properties on HIFU hyperthermia: A numerical simulation study. Applied Sciences. 2018 Oct 16;8(10):1933. doi:10.3390/app8101933.
- 7. Wang M, Lei Y, Zhou Y. High-intensity focused ultrasound (HIFU) ablation by the frequency chirps: Enhanced thermal field and cavitation at the focus. Ultrasonics. 2019;91:134-49. doi:10.1016/j.ultras.2018.08.017.
- 8. Zou X, Dong H, Qian SY. Influence of dynamic tissue properties on temperature elevation and lesions during HIFU scanning therapy: Numerical

- simulation. Chin Phys B. 2020;29(3):034305. doi:10.1088/1674-1056/29/3/034305.
- Takagi R, Yoshinaka K, Washio T, Koseki Y. A visualization method for a wide range of rising temperature induced by high-intensity focused ultrasound using a tissue-mimicking phantom. International Journal of Hyperthermia. 2022 Dec 31;39(1):22-33. doi:10.1080/02656836.2021.1942324.
- Li C, Chen S, Wang Q, Li H, Xiao S, Li F. Effects of thermal relaxation on temperature elevation in ex vivo tissues during high intensity focused ultrasound. IEEE Access. 2020 Nov 24;8:212013-21. doi:10.1109/ACCESS.2020.3028991.
- 11. Dong H, Liu G, Peng G. Numerical simulation of the effect of temperature-dependent acoustic and thermal parameters on the focal temperature and thermal lesion of biological tissue irradiated by HIFU. Iran J Med Phys. 2023;20(5):257-65. doi:10.22038/IJMP.2022.65642.2126.
- Luan S, Ji Y, Liu Y, Zhu L, Zhou H, Ouyang J, Yang X, Zhao H, Zhu B. Real-time reconstruction of HIFU focal temperature field based on deep learning. BME frontiers. 2024 Mar 21;5:0037. doi:10.1007/s43317-024-0037-5.
- 13. Xu P, Wu H, Shen G. Characterization of weakly nonlinear effects in relationship to transducer parameters in focused ultrasound therapy. Med Phys. 2024;51(10):7619-31. doi:10.1002/mp.12723.
- Zheng Y, Maev RG, Solodov IY. Nonlinear acoustic applications for material characterization: a review. Can J Phys. 2000;77(12):927-67. doi:10.1139/cjp-77-12-927.
- 15. Varray F, Ramalli A, Cachard C, Tortoli P, Basset O. Fundamental and second-harmonic ultrasound field computation of inhomogeneous nonlinear medium with a generalized angular spectrum method. IEEE transactions on ultrasonics, ferroelectrics, and frequency control. 2011 Jul 14:58(7):1366-76. doi:10.1109/TUFFC.2011.1879.
- 16. Roohi R, Baroumand S, Hosseinie R, Ahmadi G. Numerical simulation of HIFU with dual transducers: The implementation of dual-phase lag bioheat and non-linear Westervelt equations. International Communications in Heat and Mass Transfer. 2021 Jan 1;120:105002. doi:10.1016/j.icheatmasstransfer.2020.105002.
- 17. Zhao P, Wang Y, Tong S, Tao J, Sheng Y. The Effects of Energy on the Relationship between the Acoustic Focal Region and Biological Focal Region during Low-Power Cumulative HIFU Ablation. Applied Sciences. 2023 Apr 1;13(7):4492. doi:10.3390/app1374492.
- Qi M, Liu J, Mao Y, Liu X. Temperature rise induced by an annular focused transducer with a wide aperture angle in multi-layer tissue. Chinese Physics B. 2018;27(1):014301. doi:10.1088/1674-1056/27/1/014301.
- Mortazavi S, Mokhtari-Dizaji M. Numerical study of high-intensity focused ultrasound (HIFU) in fat reduction. Skin Research and Technology. 2023 Jan;29(1):e13280. doi:10.1111/srt.13280.
- Dong H, Liu G, Tong X. Influence of temperaturedependent acoustic and thermal parameters and nonlinear harmonics on the prediction of thermal lesion under HIFU ablation. Math. Biosci. Eng. 2021 Jan 1;18:1340-51. doi:10.3934/mbe.2021238.



- 21. Solovchuk MA, Hwang SC, Chang H, Thiriet M, Sheu TW. Temperature elevation by HIFU in ex vivo porcine muscle: MRI measurement and Medical simulation study. physics. May;41(5):052903. doi:10.1118/1.4869822.
- Aubry JF, Bates O, Boehm C, Butts Pauly K, Christensen D, Cueto C, et al. Benchmark problems transcranial ultrasound Intercomparison of compressional wave models. The Journal of the Acoustical Society of America. 2022 Aug 1;152(2):1003-19. doi:10.1121/10.0013426.
- Kinsey AM, Diederich CJ, Rieke V, Nau WH, Pauly KB, Bouley D, et al. Transurethral ultrasound applicators with dynamic multi-sector control for prostate thermal therapy: in vivo evaluation under guidance. Medical physics. May;35(5):2081-93. doi:10.1118/1.2900131.
- Bernard S, Kazemirad S, Cloutier G. A frequencyshift method to measure shear-wave attenuation in soft tissues. IEEE Trans Ultrason Ferroelectr Freq 2016;64(3):514-24. Control. doi:10.1109/TUFFC.2016.2541.
- Wei C, Zhang H, Fan H, Wang P, Peng D, Liu Y. Resolving high-frequency aeroacoustic noises of high-speed dual-impinging jets using fast pressuresensitive paint. Experiments in Fluids. 2024 Sep;65(9):131. doi:10.1007/s00348-024-03336-5.
- Karlinsky KT, Ilovitsh T. Ultrasound frequency mixing for enhanced contrast harmonic imaging of microbubbles. IEEE Trans Ultrason Ferroelectr Freq 2022;69(8):2414-24. doi:10.1109/TUFFC.2022.3174.
- Mortazavi S, Mokhtari-Dizaji M. Threshold of linear and non-linear behavior of high intensity focused ultrasound (HIFU) in skin, fat, and muscle tissue using computer simulation. Iran J Med Phys. 2022;19:181-8. doi:10.22038/IJMP.2021.59077.1992.
- Hussain M, Kaassamani S, Auguste T, Boutu W, Gauthier D, Kholodtsova M, et al. Spectral control of high order harmonics through non-linear propagation effects. Applied Physics Letters. 2021 Aug 16;119(7). doi:10.1063/5.1211.
- Gnawali S, Ghimire R, Magar KR, Hossaini SJ, Apalkov V. Ultrafast electron dynamics of graphene quantum dots: High harmonic generation. Physical Review В. 2022 Aug 15;106(7):075149. doi:10.1103/PhysRevB.106.075149.